

# F-GAMMA: On the phenomenological classification of continuum radio spectra variability patterns of *Fermi* blazars

E Angelakis<sup>1</sup>, L Fuhrmann<sup>1</sup>, I Nestoras<sup>1</sup>, C M Fromm<sup>1</sup>, M Perucho<sup>2</sup>,  
R Schmidt<sup>1</sup>, J A Zensus<sup>1</sup>, N Marchili<sup>1</sup>, T P Krichbaum<sup>1</sup>,  
H Ungerechts<sup>3</sup>, A Sievers<sup>3</sup>, D Riquelme<sup>3</sup> and V Pavlidou<sup>1</sup>

<sup>1</sup> Max-Planck-Institut für Radioastronomie, Auf dem Hügel 69, DE-53121, Bonn, Germany

<sup>2</sup> Department d'Astronomia i Astrofísica, Universitat de València, C/Dr. Moliner 50, 46100 Burjassot, València, Spain

<sup>3</sup> Instituto de Radio Astronomía Milimétrica, Avenida Divina Pastora 7, Local 20, E 18012, Granada, Spain

E-mail: eangelakis@mpe.mpg.de

**Abstract.** The *F-GAMMA* program is a coordinated effort to investigate the physics of Active Galactic Nuclei (AGNs) via multi-frequency monitoring of *Fermi* blazars. In the current study we show and discuss the evolution of broad-band radio spectra, which are measured at ten frequencies between 2.64 and 142 GHz using the Effelsberg 100-m and the IRAM 30-m telescopes. It is shown that any of the 78 sources studied can be classified in terms of their variability characteristics in merely 5 types of variability. It is argued that these can be attributed to only two classes of variability mechanisms. The first four types are dominated by spectral evolution and can be described by a simple two-component system composed of: (a) a steep quiescent spectral component from a large scale jet and (b) a time evolving flare component following the “Shock-in-Jet” evolutionary path. The fifth type is characterised by an achromatic change of the broad band spectrum, which could be attributed to a different mechanism, likely involving differential Doppler boosting caused by geometrical effects. Here we present the classification, the assumed physical scenario and the results of calculations that have been performed for the spectral evolution of flares.

## 1. Introduction

Among the most evident characteristics of blazars is their intense variability at all wavelengths. Studies of the variability characteristics, preferably with simultaneous data, shed light on the physics driving the energy production and dissipation in these systems (e.g. [2, 3]). The *F-GAMMA* program [4, 5, 6] explores this possibility by coordinated monthly monitoring of *Fermi*  $\gamma$ -ray monitored blazars. *F-GAMMA* is covering mostly the radio cm to sub-mm bands primarily with the Effelsberg 100-m, the IRAM 30-m and the APEX 12-m telescopes (although optical telescopes are participating as well, Fuhrmann et al. in prep.) for  $\sim 60$  prominent blazars.

The physical cause for the variability itself has been long debated. The “Shock-in-Jet” model suggested by [1], is the most accepted one and attributes the variability to shocks propagating down the jet. The basic assumption is that variations at the jet base (e.g. changes in the injection rate, the magnetic field, bulk Lorentz factor etc.) cause the formation of shocks, which

consequently go through first *Compton*, then *synchrotron* and finally *adiabatic* energy losses. This is the main model prediction which is adopted in the following.

An alternative model, the “Internal Shock Model” proposed by [7], suggests that energy is channeled into the jet in an intermittent way. “Plasma shells”, may have different bulk Lorentz factors and masses, so that faster shells can catch up with slower ones, collide and relativistic shocks can occur. The shock accelerates electrons to relativistic energies so that they can emit synchrotron and inverse Compton radiation.

Other models explain the variability geometrically. For example, [8] suggest that orbital motion and jet precession, e.g. caused by a binary black hole system, can produce helical jet morphologies which can bent the jet, changing its orientation and shape. This may then cause brightness and spectral variability through changes in the Doppler factor.

## 2. Observations

The work discussed here is based on observations conducted quasi-simultaneously with the Effelsberg 100-m and the IRAM 30-m telescope within the *F-GAMMA* program which is described in [4, 5, 6]. The 100-m telescope has been observing between 2.64 and 43.05 GHz at 8 frequencies over a baseline of 4.5 years (January 2007 – June 2011). The 30-m telescope has been measuring at 86 and 142 GHz (June 2007 – June 2011). The millimetre observations for *F-GAMMA* are closely coordinated with the more general flux monitoring conducted by IRAM, and data from both programs are included in this paper. The Effelsberg 100-m telescope is equipped with circularly polarised feeds, while the IRAM 30-m with linearly polarised ones. Details are given elsewhere (Fuhrmann et al. in prep., Angelakis et al. in prep., Nestoras et al. in prep.). Measurements at 4.85 GHz, 10.45 GHz, 32.0 GHz, 86.24 GHz and 142 GHz are done differentially either by using multi-feed systems, or, at IRAM 30-m, by wobbler switching.

On average, the time needed for observing an entire spectrum of any given source at Effelsberg alone is of the order of 35 minutes, while at IRAM, roughly 2 minutes. The combined spectra (Effelsberg and IRAM) are observed quasi-simultaneously within approximately one week. That is, neither the single-facility nor the combined spectra are likely to be affected by source variability. In the current study only data collected until June 2011, have been used.

## 3. Data reduction

The antenna temperature measured for a certain source is subjected to a series of corrections to compute the source flux density outside the terrestrial atmosphere. These operations, are: (a) *Pointing correction*, meant to correct for small pointing residuals. (b) *Elevation dependent gain correction*, correcting for the loss of antenna sensitivity caused by gravitational deformation of the reflector. (c) *Atmospheric opacity correction*, which corrects for the attenuation due to the terrestrial atmospheric absorption. (d) *Absolute calibration (sensitivity correction)*, which does the translation of the previously corrected antenna temperature to SI units. All measurements are subsequently exposed to quality checks. The overall uncertainties are typically of the order of 0.5 – 5 % for Effelsberg and of the order of  $\leq 10\%$  for IRAM. More details can be found in [9] as well as in Angelakis et al. (in prep.) and in Nestoras et al. (in prep.).

## 4. Phenomenological classification of the spectrum variability pattern

The following discussion refers to the phenomenological classification of the variability patterns shown by the broad-band spectra of sources in the *F-GAMMA* sample relative to the observing band-pass. The term “variability pattern” is assigned to the shape traced by the source broad-band spectrum – as that is observed monthly – as a function of time. In total 78 sources have been examined and their spectra span, in total, over 4.5 years of observations.

A visual inspection of the examined sources reveals a wealth of spectral features as well as of variability patterns that different sources exhibit. For instance, the variability amplitude,

the frequency of occurrences and the pace at which the variability events evolve, seem to be different for different sources. Interestingly, despite the apparent complexity it appears that the 78 sources that have been studied here can be classified in only five phenomenological classes on the basis of its variability pattern, which are numbered from 1 to 5 (more details will be given by Angelakis et al. in prep.). Four of them show also sub-types which however do not deserve a separate type and are named after the main type followed by the letter “b”. The prototype sources are shown in figures 2–10. The main phenomenological characteristics of these types, are:

**Type 1** : This variability pattern is clearly dominated by spectral evolution. That is, at an instant of time the spectrum appears convex and its peak ( $S_m, \nu_m$ ) is drifting within the observing band-pass from high towards lower frequencies, covering a significant area in the  $S - \nu$  space. Its shape is smoothly changing towards an ultimate flat or mildly steep power law which is then followed by new events. For this type no evidence for the presence of an underlying quiescent steep spectrum is seen. The lowest frequencies in the bandpass are remarkably variable indicating that the activity ceases at frequencies much lower than the lowest in our band-pass. The prototype source is shown in figure. 2.

**Type 1b** : As a sub-class of the previous one, type 1b shares the same characteristics with type 1 except that the lowest frequency does not show as intense a variability. The activity ceases around this part of the band-pass. A source representative of this type is shown in figure 3.

**Type 2** : This type is also dominated by spectral evolution. The basic characteristic of this case is the fact that the flux density at the lowest frequency during the steepest spectrum phase is higher than that during the inverted spectrum phase. Moreover, the maximum flux density reached by the flaring events is significantly above that at the lowest frequency. This implies that the observed steep spectrum is not a quiescent spectrum but rather the relic of an older, yet recent, outburst. The prototype of this type is shown in figure 4.

**Type 3** : Type 3, shown in figure 5, is dominated by the spectral evolution as well. The identifying characteristics, are: (a) the fact that the lowest frequency practically does not vary and, (b) the maximum flux density level reached by outbursts is comparable to that at the lowest band-pass frequency. This phenomenology leaves hints that the events cease very close to the lowest frequency of the band-pass and hence a quiescent spectrum is becoming barely evident.

**Type 3b** : Type 3b, shown in figure 6, is very similar to type 3. Here however the quiescent spectrum is seen clearly at least at the 2 lowest frequencies.

**Type 4** : Sources of this type spend most of the time as steep spectrum ones which are sometimes showing an outburst of relatively low power propagating towards low frequencies. A representative case is shown in figure 7.

**Type 4b** : This type includes persistently steep spectrum cases as it is shown in figure 8.

In all previous classes, type 1 to 4b, the occurring variability is clearly dominated by spectral evolution. However, there exists a class of sources that show a fundamentally different behaviour. The variability happens self-similarly without signs of spectral evolution. Those are grouped in a separate type with two sub-types:

**Type 5** : In this case the spectrum is convex and follows an “achromatic” evolution. That is, it shifts its position in the  $S - \nu$  space preserving its shape. This is shown clearly in figure 9.

**Type 5b** : This type shows, in principle, characteristics similar to the previous one but there occurs a mild yet noticeable shift of the peak ( $S_m, \nu_m$ ) towards lower frequencies as the peak flux density increases. A characteristic case is shown in figure 10.

The distribution of sources over the different variability types are shown in figure 1. The sub-classes with the label “b” are numbered with appending the fraction 0.5 to the numerical tag of the corresponding type (e.g. Type 5b appears as 5.5). As can be seen, the majority of the sources show variability of type 1 – 3b which is the result of the *F-GAMMA* sample selection (i.e. sources variable at all frequencies). Interestingly, a small number of sources (eight) show it is discussed later.

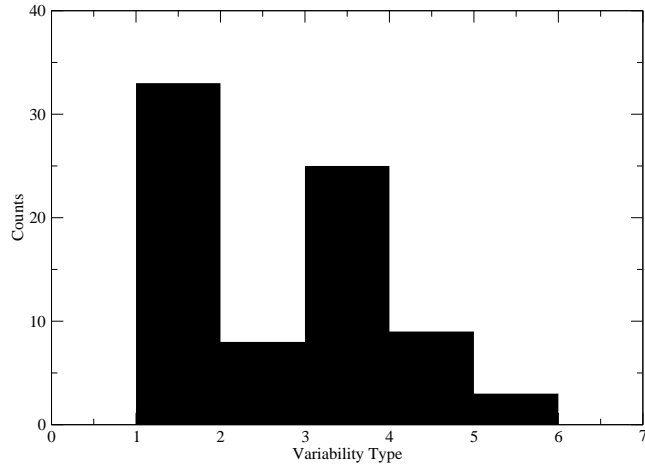


**Figure 1.** The distribution of sources over spectral variability type. The sub-classes labeled “b” are enumerated with appending .5 to the class number. For example, 5b should appear as 5.5. The number of sources used here are 78.

This classification is done solely on the basis of the phenomenological characteristics of the variability pattern shown by the radio spectra within a given band-pass. As it is discussed in the next section, it appears that all the phenomenology for types 1–4b can be naturally explained by the same physical system observed under different circumstances.

## 5. A physical interpretation of the variability types

In the following it is suggested that the classification discussed earlier can be reproduced by a simple two-component system observed under different circumstances.

Let us assume a simple two-component system at  $z = 0$ , consisted of:

- (i) A power-law quiescent spectrum with  $S \propto \nu^\alpha$  (e.g.  $\alpha \approx -0.5$ ). This can be attributed to the optically thin diffuse emission of a large scale jet or even relic recent flaring event or blends of such.
- (ii) A convex synchrotron self-absorbed spectrum (hereafter SSA) representative of a recent outburst superimposed on the quiescent part.

The assumed configuration is presented in figure 11 where the shaded areas denote the observing band-pass. The phenomenology shown there captures the system (solid line) at an instant in time. Consequently the spectral shape that would be observed at that instant of time would depend on two parameters of the shaded areas (band-pass) shown there:

- (i) The **position** of the shaded areas relative to the high and low frequency peak of the assumed system. This parameter denotes the relative position of the centre of our band-pass with respect to the source spectrum.
- (ii) The **width** of the shaded areas relative to the width of the bridge between the optically thick part of the outburst and the steep part of the quiescent spectrum. This parameter denotes the fraction of the spectrum that the band-pass can sample.

Within this scenario it can be said that as the variability type increases the dominance of the steep quiescent spectrum becomes progressively larger and the basic characteristics of the

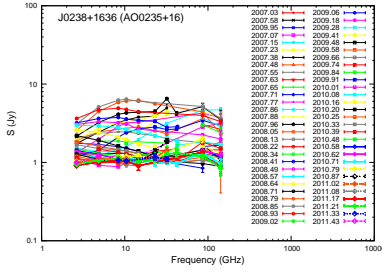


**Figure 2.** Prototype source for variability type 1.

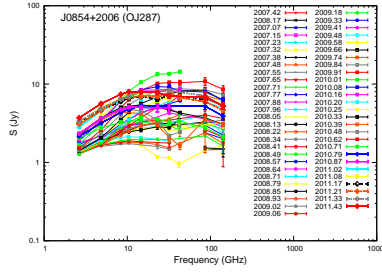


**Figure 3.** Prototype source for variability type 1b.

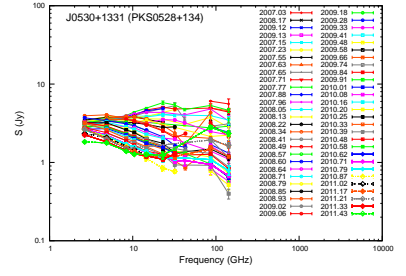


**Figure 4.** Prototype source for variability type 2.

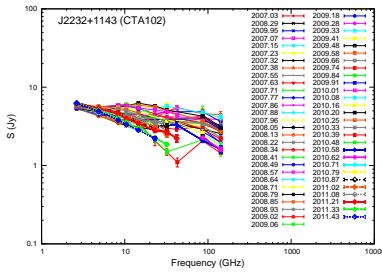


**Figure 5.** Prototype source for variability type 3.

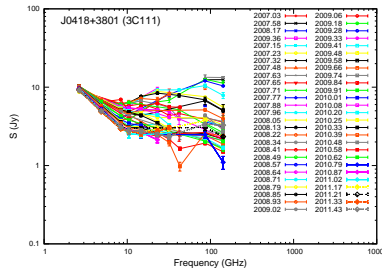


**Figure 6.** Prototype source for variability type 3b.

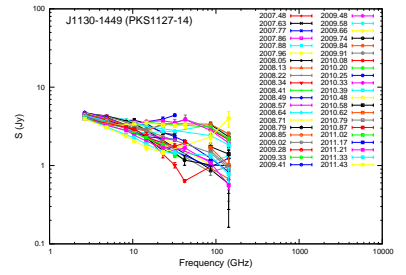


**Figure 7.** Prototype source for variability type 4.

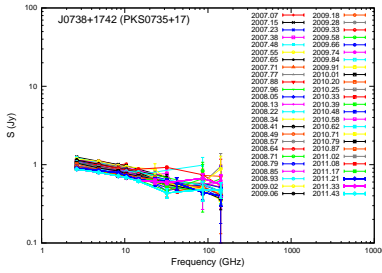


**Figure 8.** Prototype source for variability type 4b.

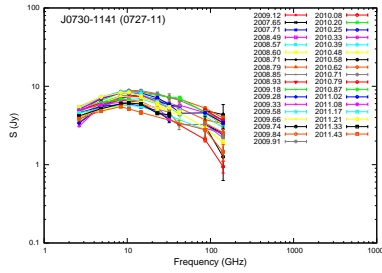


**Figure 9.** Prototype source for variability type 5.

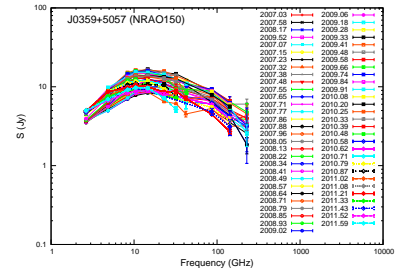


**Figure 10.** Prototype source for variability type 5b.

observed variability types 1–4b can be reproduced naturally with the appropriate modulation of these two parameters.

The question that naturally arises then is how can these two quantities be modulated. Qualitatively speaking, this can be formulated in terms of the combination of (a) *redshift* and (b) *source intrinsic properties*. The *redshift* changes the relative *position* of the band-pass allowing a different part of the spectrum to be sampled. The *source intrinsic properties* imply that different sources show different spectral characteristics, such as: peak frequency of the outburst, peak flux density excess of the outburst relative to the quiescent spectrum, different broadness of the valley, different broadness of the SSA spectrum of the outburst etc. Accounting now for the dynamical evolution of a flaring event in the  $S_m - \nu_m$  space, one can introduce a third factor namely (c) the *flare specific properties* which of course are also a function of the *source intrinsic properties* and allow the system to evolve dynamically. While factors (a) and (b) have a static effect and determine the general shape of the observed spectrum, the latter one (c) changes both the relative position and width of the band-pass dynamically shaping the specific

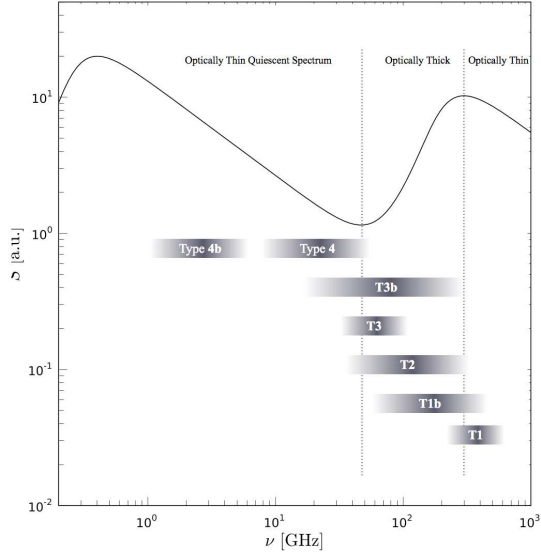


**Figure 11.** The assumed common underlying two-component system. The different variability types can be reproduced with the appropriate modulation of the relative position and relative broadness of the band-pass denoted by the grey shaded areas.

characteristics of the variability pattern. In the following we present calculations that have been done to examine whether this scenario can reproduce the observed phenomenologies.

## 6. Modelling the broad band radio spectra

Following the hypothesis that all the observed events are the reflection of the same process, namely shocks evolving in jets seen with different frequency band-passes at different evolutionary stages, the Shock-in-Jet model [1, 10] has been applied to reproduce their temporal evolution.

Specifically, our approach is presented in [11], and relies on the information extracted from the quiescent spectrum and the flaring event to connect the different radiative evolutionary stages of the shock (*Compton*, *Synchrotron* and *Adiabatic* stage). The distribution of the quiescent spectrum parameters depends on the intrinsic source properties such as the magnetic field in the jet,  $B$ , the Doppler factor,  $D$ , and the normalisation coefficient of the spectrum,  $K$ . The spectral behaviour of the injected component, depends on the evolution of the physical parameters of the shock and is parametrized by the exponents in the relations giving  $B$ ,  $K$  and  $D$  as functions of the distance along the jet:  $L \propto R^r$ ,  $B \propto L^{-r \cdot b}$ ,  $K \propto L^{-r \cdot k}$ ,  $D \propto L^{-r \cdot d}$ , where  $r$  is the opening rate of the jet. In the current work it is assumed that the *Synchrotron* stage is very short compared to the other two stages (see [11]).

We have calculated the spectral evolution of flares for three characteristic cases in terms of source *luminosity*: weak, medium and strong and for three *redshifts*: 0, 1.5 and 3. In every case the peak flux of the flaring event at time 0 was set equal to the turnover flux of the quiescent spectrum. Subsequently the flare has been left to evolve according to the evolutionary model discussed previously ([1, 10, 11]). Figures 12–20 show the spectra expected to be observed by a facility with band-pass of 2–140 GHz (*F-GAMMA* program). It is evident from there that the majority of the types discussed earlier are reproduced naturally. Elsewhere (Angelakis et al. in prep.) more cases are simulated increasing the expected variability patterns.

## 7. Discussion

From the discussion in section 4, it is evident that the variability phenomenologies of the studied blazars can be categorised in two fundamentally different classes. (a) Sources that are dominated by spectral evolution and (b) sources that have a convex spectrum and vary self-similarly with only mild if at all spectral evolution. This implies that there must exist two distinct mechanisms causing variability. It must be noted though that this refers to the available baseline (roughly

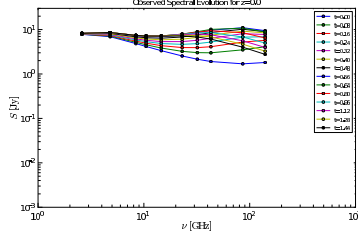


**Figure 12.** The spectrum expected from a powerful source at  $z = 0$ .

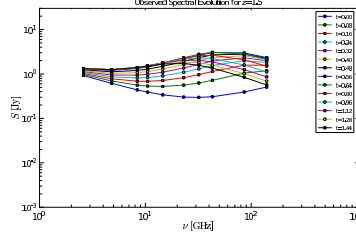


**Figure 13.** The spectrum expected from a powerful source at  $z = 1.5$ .

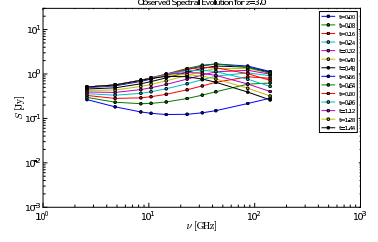


**Figure 14.** The spectrum expected from a powerful source at  $z = 3.0$ .

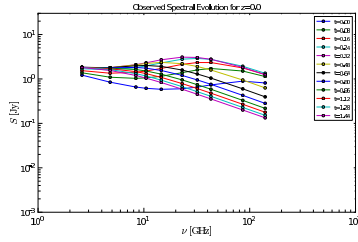


**Figure 15.** The spectrum expected from a medium source at  $z = 0$ .

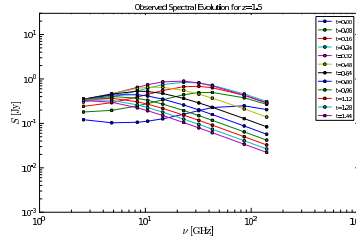


**Figure 16.** The spectrum expected from a medium source at  $z = 1.5$ .

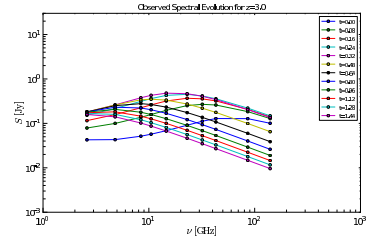


**Figure 17.** The spectrum expected from a medium source at  $z = 3.0$ .

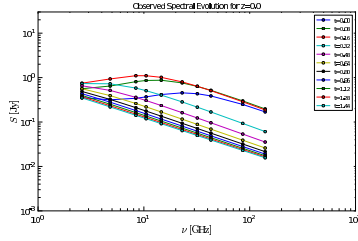


**Figure 18.** The spectrum expected from a weak source at  $z = 0$ .

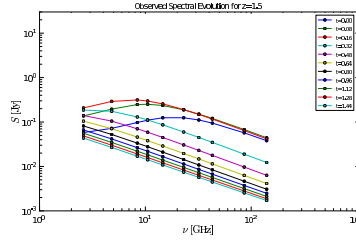


**Figure 19.** The spectrum expected from a weak source at  $z = 1.5$ .

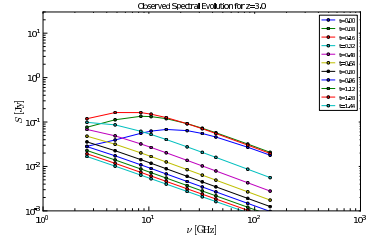


**Figure 20.** The spectrum expected from a weak source at  $z = 3.0$ .

five years) meaning that sources of type 5 and 5b could still show spectral evolution over longer time scales. An additional element that points towards a different variability mechanism is the persistency of the spectral shape, in the case of type 5 and the fashion of change in the case of type 5b which is not seen in cases of clear spectral evolution.

Of the 78 sources that have been examined for the current work, 8 show achromatic variability. The interesting characteristic is that in the cases that show a mild spectral evolution, the turnover flux and frequency  $S_m$  and  $\nu_m$ , are evolving in an anti-correlated fashion (see e.g. figure 10). Apart from the fact that all of them show the clear presence of a large scale jet even at 2 cm (as it is shown from the MOJAVE images [12]) no other peculiar property has been identified so far. Possible mechanisms that are currently investigated, include: changes in the magnetic field structure, changes in the Doppler factors and geometrical effects.

It is noteworthy that none of the studied sources has shown a switch of type at least over the

baseline of the *F-GAMMA* program, neither between types of the same underlying mechanism (i.e. 1–4b) nor between types with different underlying mechanism (i.e. types 1–4b and types 5, 5b). This suggests that the mechanism producing the variability is, either a fingerprint characteristic of the source, or the conditions that determine it change over longer time scales, if at all. Possible switch from achromatic to an evolution dominated behaviour would imply that the suggested dichotomy of the variability mechanisms is not valid. In any case, the persistency of the evolution dominated types implies that the power deposited in each event for a certain source is not varying significantly from one event to the other. Further investigations to explore this statement are underway and will be presented elsewhere.

Concerning the evolution dominated case, it seems that the Marscher & Gear model [1] provides a precise reproduction of the observed phenomenology and most importantly, over a range of intrinsic parameters covered by the *F-GAMMA* sample. Studies to examine whether other variability mechanisms can reproduce the observed phenomenology (shapes, time scales etc.) are needed. In any case, any successful model could be used for extracting the physical parameters from the observed spectra.

## Acknowledgments

Based on observations with the 100m telescope of the MPIfR (Max-Planck-Institut für Radioastronomie). Based on observations carried out with the IRAM 30m Telescope. IRAM is supported by INSU/CNRS (France), MPG (Germany) and IGN (Spain). I. Nestoras and R. Schmidt are members of the International Max Planck Research School (IMPRS) for Astronomy and Astrophysics at the Universities of Bonn and Cologne. The *F-GAMMA* team sincerely thanks the Time Allocation Committee of the 100-m and 30-m telescope for supporting the continuation of the program. E. Angelakis feels obliged to wholeheartedly thank Dr. A. Kraus for the constant support and the very constructive discussions.

## References

- [1] Marscher A P and Gear W K 1985 *ApJ* **298** 114–127
- [2] Boettcher M 2010 *ArXiv e-prints (Preprint 1006.5048)*
- [3] Boettcher M and Dermer C D 2010 *Bulletin of the American Astronomical Society (Bulletin of the American Astronomical Society vol 42)* pp 706–+
- [4] Fuhrmann L, Zensus J A, Krichbaum T P, Angelakis E and Readhead A C S 2007 *The First GLAST Symposium (American Institute of Physics Conference Series vol 921)* ed Ritz S, Michelson P and Meegan C A pp 249–251
- [5] Angelakis E, Fuhrmann L, Marchili N, Krichbaum T P and Zensus J A 2008 *Memorie della Societa Astronomica Italiana* **79** 1042–+ (*Preprint 0809.3912*)
- [6] Angelakis E, Fuhrmann L, Nestoras I, Zensus J A, Marchili N, Pavlidou V and Krichbaum T P 2010 *ArXiv e-prints (Preprint 1006.5610)*
- [7] Spada M, Ghisellini G, Lazzati D and Celotti A 2001 *MNRAS* **325** 1559–1570 (*Preprint arXiv:astro-ph/0103424*)
- [8] Villata M and Raiteri C M 1999 *A&A* **347** 30–36
- [9] Angelakis E, Kraus A, Readhead A C S, Zensus J A, Bustos R, Krichbaum T P, Witzel A and Pearson T J 2009 *A&A* **501** 801–812 (*Preprint 0905.2660*)
- [10] Türler M, Courvoisier T and Paltani S 2000 *A&A* **361** 850–862 (*Preprint arXiv:astro-ph/0008480*)
- [11] Fromm C M, Perucho M, Ros E, Savolainen T, Lobanov A P, Zensus J A, Aller M F, Aller H D, Gurwell M A and Lähteenmäki A 2011 *A&A* **531** A95+ (*Preprint 1105.5024*)
- [12] Kellermann K I, Lister M L, Homan D C, Vermeulen R C, Cohen M H, Ros E, Kadler M, Zensus J A and Kovalev Y Y 2004 *ApJ* **609** 539–563 (*Preprint astro-ph/0403320*)